Modeling Solid Oxide Fuel Cells Using Continuous-Time Recurrent Fuzzy Systems

A. Flemming , J. Adamy *

Darmstadt University of Technology, Institute for Automatic Control, Landgraf-Georg-Strae 4, 64283 Darmstadt, Germany

Abstract

Continuous-time recurrent fuzzy systems allow modeling continuous-time processes whose dynamic behavior can be stated in linguistic if-then rules. If the dynamics are known in certain mesh points, the interpolating character of the fuzzy system between the mesh points yields a complete dynamical model of the process. In this contribution, continuous-time recurrent fuzzy systems are employed to model the electrical behavior of a solid oxide fuel cell, which both can be described qualitatively and is known quantitatively from measurements. Due to the transparency of the model an easy estimation of its parameters is possible. Additionally, the model parameters are optimized numerically to enhance the model performance.

Key words: Solid oxide fuel cell, continuous-time recurrent fuzzy system, nonlinear time-variant model, qualitative modeling

1. Introduction

Fuel cells offer an energy source that is independent of fossil fuels and has low emissions, so that they are a promising energy conversion device. Different types of fuel cells have been developed. Fig. 1 gives an overview of common fuel cell types, which, e.g., employ different electrolyte materials, differ in their operating temperature, and use different charge carriers (Larminie and Dicks, 2003; O'Hayre *et al.*, 2006). In the following, we only consider solid oxide fuel cells (SOFC).

For the analysis and enhancement of SOFC and systems incorporating them, models were developed describing the different dynamical effects that appear, e.g., chemical effects, thermodynamical effects, and electrical effects. Models of SOFC that can be found in literature are, e.g., dynamical models based on electrochemical and thermodynamical effects (Sedghisigarchi and Feliachi, 2004; Gemmen and Johnson, 2005; Ota *et al.*, 2003; Achenbach, 1995; Hall and Colclaser, 1999; Lu *et al.*, 2006; Qi *et al.*, 2005, 2006; Xu *et al.*, 2006; Padullé *et al.*, 2000). Some are complex state space models (Lu *et al.*, 2006; Qi *et al.*, 2005, 2006). Other dynamical models consider the incorporation into a large power system (Xu *et al.*, 2006; Padullé *et al.*, 2000; Ivers-Tiffée *et al.*, 2004). By using numerical methods, dynamical models were developed in Ivers-Tiffée *et al.* (2004); Jurado (2004*b*); Jurado *et al.* (2004); Jurado (2004*a*); Haschka *et al.* (2006).

type	electrolyte	operating temp.	charge carrier
SOFC	ceramic	$600 - 1000°C$	O^{2-}
PEMFC	polymer membrane	$80°C$	H^+
PAFC	liquid H_3PO_4	$200°C$	H^+
AFC	liquid KOH	$60 - 220°C$	OH^-
MCFC	molten carbonate	$650°C$	CO_3^{2-}

Fig. 1. Major fuel cell types.

Unfortunately, the micro scale models require detailed knowledge of the electrochemical and thermodynamical effects that appear in SOFC. Macro scale models, which can be used within a large power system model, allow a higher level of abstraction (Ivers-Tiffée *et al.*, 2004). In this case, it is of interest to model the dynamic input-output characteristics of the fuel cell. Thus, they do not require the incorporation of all known physical properties. However, models solely using numerical methods, i.e. black box models, are not transparent and do not allow to incorporate expert knowledge in the form of linguistic rules. In Ivers-Tiffée *et al.* (2004) a dynamical macro scale model, combining qualitative expert knowledge with physical properties and measured data, that allows simulating the start-up of a SOFC was developed.

* Corresponding author. Tel. +49-(0)6151-16-3442. Fax +49-(0)6151-16-2507.

Email address: `adamy@rtr.tu-darmstadt.de` (, J. Adamy).

[1] This work was supported by the government of the state of Hesse, Germany, under grant no. 011206.

The aim of this work is the proposition of a macro scale SOFC model describing the dynamic interrelationship between the current density and the voltage loss during the operation of a SOFC. The model exploits the fact that the different dynamic and static voltage losses, which occur in the fuel cell, can be qualitatively described using if-then rules. By employing continuous-time recurrent fuzzy systems, a mathematical dynamic model is derived from the qualitative linguistic model. In contrast to Sedghisigarchi and Feliachi (2004); Gemmen and Johnson (2005); Ota *et al.* (2003); Achenbach (1995); Hall and Colclaser (1999); Lu *et al.* (2006); Qi *et al.* (2005, 2006); Xu *et al.* (2006); Padullé *et al.* (2000); Jurado (2004*b*); Jurado *et al.* (2004); Jurado (2004*a*); Haschka *et al.* (2006), the proposed model is transparent, i.e., interpretable. Due to its transparency, good model parameters are estimated heuristically from measured data without numerical identification methods.

Furthermore, it is possible to observe that the characteristics of the electrical behavior of the SOFC changes during its operation time. Thus, the degradation process is included into the model, which leads to a time-variant model.

The article is organized as follows: in Section 2, the operation mode of SOFC is elucidated. An introduction to continuous-time recurrent fuzzy systems is given in Section 3. The qualitative and quantitative model of the electrical behavior of SOFC using continuous-time recurrent fuzzy systems is proposed in Section 4 and Section 5, respectively. Subsequently, Section 6 presents the simulation results employing this model. The degradation process of the fuel cell is incorporated into the model in Section 7. Section 8 presents the simulation results of this time-variant model. Finally, a conclusion is given in Section 9.

2. Operation mode of solid oxide fuel cells

In general, fuel cells exploit the chemical reaction of hydrogen and oxygen, which is known as detonating gas reaction. In the case of a fuel cell, both reactants, i.e., the oxygen at the cathode and the hydrogen at the anode, are separated by an electrolyte, which is only ionic permeable. In the case of a SOFC the electrolyte consists of a solid ceramic material. Due to the spatial separation of oxygen and hydrogen, the electron transfer that occurs during the reaction of the two reactants, can be harnessed as an electrical current (Larminie and Dicks, 2003; O'Hayre *et al.*, 2006).

The reaction proceeds in two electrochemical half reactions as follows: The oxygen absorbs free electrons at the cathode according to the chemical reaction

$$\frac{1}{2}O_2 + 2e^- \rightarrow O^{2-}$$

and passes the electrolyte in ionic form. At the anode, the oxygen ions release their electrons during the reaction with the hydrogen according to

$$O^{2-} + H_2 \rightarrow H_2O + 2e^-,$$

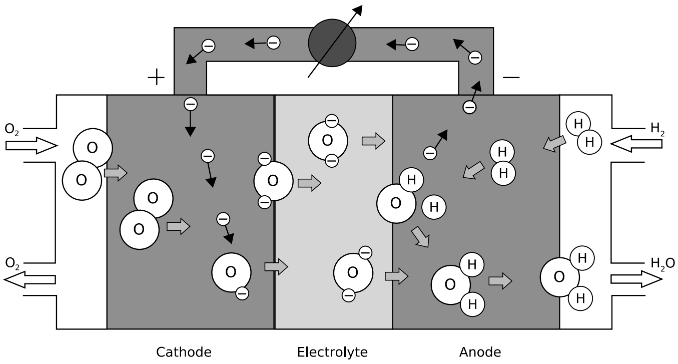

Fig. 2. Scheme of a SOFC. The white circles symbolize the electrons.

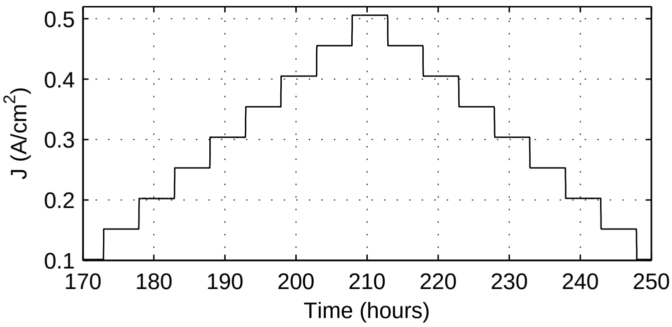

Fig. 3. Measurements of the current density J.

which yields water and free electrons. The free electrons at the anode can be harnessed by transporting them back to the cathode through a conductor, which is connected to a consumer load (Larminie and Dicks, 2003; O'Hayre *et al.*, 2006). Fig. 2 shows a scheme of a SOFC.

The reactions take place where the highly porous electrodes allow intimate contact between the three phases gas, electrically conductive electrode, and ion-conductive electrolyte. These reaction sites are denoted as triple phase boundaries (O'Hayre *et al.*, 2006).

The theoretical possible cell voltage of 1.229V at the output of the fuel cell (O'Hayre *et al.*, 2006), which is determined for the thermodynamical equilibrium, i.e., without a current flow, cannot be achieved in practice due to several loss effects. These effects lead to a voltage loss U_V, which increases with increasing current density, J, i.e., with decreasing consumer load. The voltage loss, U_V, depending on the current density, J, is a characteristic parameter of the SOFC (Larminie and Dicks, 2003; O'Hayre *et al.*, 2006). Fig. 3 shows measurements of the current density, J, and Fig. 4 presents the measurements of the resulting voltage loss, U_V of an SOFC.

The overall voltage loss, U_V, arises from static and dynamic voltage losses, which are elucidated in the next subsection.

2.1. *Static and dynamic voltage losses*

The static voltage loss, U_s, that arises in the operation mode with constant current density, J, can be ascribed to three different effects. First, there exists an ohmic voltage

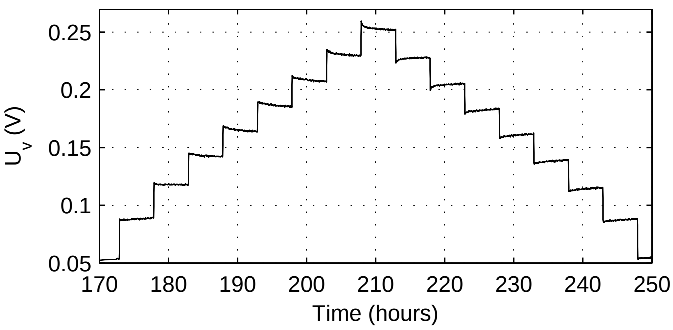

Fig. 4. Measurements of the voltage loss U_V.

drop due to the transport of electrons and ions. This voltage loss linearly increases with increasing current density.

The second effect occurs at the triple phase boundary between the cathode and the electrolyte where energy is necessary to dissociate oxygen molecules, ionize them and to transport them over the phase boundary into the electrolyte. This effect is called activation polarization. The resulting voltage loss depends nonlinearly on small current densities and approximately linearly on higher current densities (Haschka *et al.*, 2006; Larminie and Dicks, 2003; O'Hayre *et al.*, 2006).

The third effect is called gas diffusion polarization and arises especially when high current densities occur. It appears because the necessary oxygen at the cathode is taken from the air, such that oxygen has to diffuse from the surrounding air to the cathode at a sufficient rate to meet the requirements of the electrochemical reaction. The reduction in reactant concentration leads to a voltage loss. The impact of this effect on the overall static voltage loss is small in comparison to the first two effects (Haschka *et al.*, 2006; Larminie and Dicks, 2003; O'Hayre *et al.*, 2006).

In addition to the effects that cause a static voltage loss, there exists also a dynamic voltage loss U_d, which is the result of two different effects. These effects appear when a change, $\dot{J}$, in current density occurs and also depend on the value of the current density, J.

The first of these two effects is called temperature effect and is caused by the current density change, which leads to a temperature alteration and hereupon to a conductivity change. The time constant of this effect is approximately 3-5 minutes (Haschka *et al.*, 2006; Larminie and Dicks, 2003; O'Hayre *et al.*, 2006).

The second dynamic effect appears at the cathode where the oxygen is dissociated, ionized and transported into the electrolyte. This triple phase boundary cannot immediately adapt to a change in the current density. Thus, if the current density rises, the local current density at the triple phase boundary increases, which yields a higher voltage loss. After some time has passed, the triple phase boundary grows, such that the local current density reduces to the previous value. The reverse case occurs if the current density decreases. This effect is called structural effect and its time constant is approximately 1-5 hours (Haschka *et al.*, 2006; Larminie and Dicks, 2003; O'Hayre *et al.*, 2006). The overall voltage loss, U_V, is the sum of the voltage losses U_s and U_d.

The characteristics of the static and dynamic effects causing U_s and U_d also depend on the length of the operation period of the SOFC, i.e., the SOFC degrades during operation (Larminie and Dicks, 2003; O'Hayre *et al.*, 2006). The reasons for this deterioration are elucidated in the following paragraph.

2.2. *Change of voltage loss due to deterioration*

The deterioration of the SOFC during operation is caused by many different influencing factors, e.g., electrochemical effects and material effects caused by the operation of the fuel cell, which lead to a modified static and dynamical behavior of the fuel cell.

An increase of the current density, J, i.e., a positive $\dot{J}$, and therefore a positive dynamic voltage loss, U_d, has a higher influence on the degradation of a SOFC than a constant current density. This can be explained by considering the structural effect. An increase in current density leads to a local high current density at the triple phase boundary, since it cannot adopt instantaneously. The triple phase boundary increases with a slow time-constant until the local current density reduces to the previous value. The local high current density during the settling-time causes a large degradation of the material during this period (Haschka *et al.*, 2006).

During the operation with constant current densities the degradation of the material is lower. The deterioration of the fuel cell mostly leads to an increase in the ohmic voltage drop, but also leads to larger dynamical voltages losses.

3. Continuous-time recurrent fuzzy systems

The described electrical behavior of a SOFC is modeled using continuous-time recurrent fuzzy systems. A detailed description of these systems is given in Adamy and Flemming (2006). To simplify matters, a short introduction to continuous-time recurrent fuzzy systems is given in the following.

3.1. *Formal system description*

The structure of a continuous-time recurrent fuzzy system [2] is shown in Fig. 5. It comprises the complete fuzzy systems $\mathbf{f}$ and $\mathbf{g}$, i.e., they include fuzzification, inference, and defuzzification. Its inputs are the crisp state vector $\mathbf{x}(t)$ and the crisp input vector $\mathbf{u}(t)$ at a particular time t. For these inputs the crisp derivative of the state vector, $\dot{\mathbf{x}}(t)$, is computed at the output of the fuzzy function $\mathbf{f}$ and fed

[2] Continuous-time recurrent fuzzy systems are related to discrete-time recurrent fuzzy systems (Gorrini and Bersini, 1994; Adamy, 1995; Adamy and Kempf, 2003, 2004).

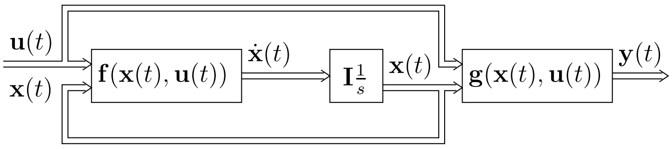

Fig. 5. Block schematic of a continuous-time recurrent fuzzy system, where f and g are fuzzy functions with fuzzification, inference, and defuzzification.

back to the input of the fuzzy function $\mathbf{f}$ through an integrator element.

The rules, which linguistically describe the dynamics of the process have the following formal form:

$$\begin{array}{lllll} \text{If} & x_1(t) = L^{x_1}_{j_1} & \text{and} \ldots \text{and} & x_n(t) = L^{x_n}_{j_n}, & \\ \text{and} & u_1(t) = L^{u_1}_{q_1} & \text{and} \ldots \text{and} & u_m(t) = L^{u_m}_{q_m}, & (1) \\ \text{then} & \dot{x}_1(t) = L^{\dot{x}_1}_{w_1(\mathbf{j},\mathbf{q})} & \text{and} \ldots \text{and} & \dot{x}_n(t) = L^{\dot{x}_n}_{w_n(\mathbf{j},\mathbf{q})}, & \end{array}$$

where $L^{x_i}_{j_i}$, $L^{u_p}_{q_p}$ and $L^{\dot{x}_i}_{w_i(\mathbf{j},\mathbf{q})}$ are the linguistic values of the linguistic states x_i, linguistic inputs u_p, and the linguistic derivatives $\dot{x}_i$, respectively. Systems with such a linguistic description have already been used in Badard and Pontet (1997); di Sciascio and Carelli (1996) without denoting them continuous-time recurrent fuzzy systems.

Each rule defines a mapping of both the index vector $\mathbf{j} = (j_1, \ldots, j_n)^T$ and the index vector $\mathbf{q} = (q_1, \ldots, q_m)^T$ onto the component w_i of an index vector $\mathbf{w} = (w_1, \ldots, w_n)^T$ indicated by the index $w_i(\mathbf{j}, \mathbf{q})$. The linguistic derivative $L^{\dot{x}_i}_{w_i(\mathbf{j},\mathbf{q})}$ indicates the change in the linguistic state x_i, i.e., it linguistically indicates whether $\dot{x}_i$ is , e.g., "positive", "negative" or "zero."

The linguistic values and linguistic derivatives can be combined into linguistic vectors $\mathbf{L}^{\mathbf{x}}_{\mathbf{j}}$, $\mathbf{L}^{\mathbf{u}}_{\mathbf{q}}$, and a linguistic gradient $\mathbf{L}^{\dot{\mathbf{x}}}_{\mathbf{w}(\mathbf{j},\mathbf{q})}$ representing the "and" correlation of their respective components, i.e., the expression $\mathbf{x} = \mathbf{L}^{\mathbf{x}}_{\mathbf{j}} = (L^{x_1}_{j_1}, \ldots, L^{x_n}_{j_n})^T$ is the short form of "$x_1 = L^{x_1}_{j_1}$ and … and $x_n = L^{x_n}_{j_n}$." This leads for each rule to the following short form:

$$\text{If } \mathbf{x}(t) = \mathbf{L}^{\mathbf{x}}_{\mathbf{j}} \text{ and } \mathbf{u}(t) = \mathbf{L}^{\mathbf{u}}_{\mathbf{q}}, \text{ then } \dot{\mathbf{x}}(t) = \mathbf{L}^{\dot{\mathbf{x}}}_{\mathbf{w}(\mathbf{j},\mathbf{q})}. \quad (2)$$

This linguistic representation of a continuous-time recurrent fuzzy system may be formalized mathematically by employing the fuzzy function $\mathbf{f}$ and the fuzzy function $\mathbf{g}$, where

$$\dot{\mathbf{x}}(t) = \mathbf{f}(\mathbf{x}(t), \mathbf{u}(t)), \quad (3)$$

$$\mathbf{y}(t) = \mathbf{g}(\mathbf{x}(t), \mathbf{u}(t)). \quad (4)$$

The fuzzy functions $\mathbf{f}$ and $\mathbf{g}$ covering fuzzification, inference, and defuzzification allow mathematical processing and investigation of the linguistic rules.

To obtain the fuzzy function $\mathbf{f}$, membership functions, $\mu^{x_i}_{j_i}(x_i)$, are assigned to every linguistic value, $L^{x_i}_{j_i}$, of each state, x_i, on an interval $X_i \subseteq \mathbb{R}$. Each membership function takes on its maximum value at a so-called core position, $s^{x_i}_{j_i}$. The membership functions $\mu^{u_p}_{q_p}(u_p)$ and core positions $s^{u_p}_{q_p}$ are defined similarly. Singletons, $s^{\dot{x}_i}_{w_i(\mathbf{j},\mathbf{q})}$, are employed as membership functions for the linguistic values, $L^{\dot{x}_i}_{w_i(\mathbf{j},\mathbf{q})}$, of the linguistic derivatives, $\dot{x}_i$. These are the so-called core position derivatives.

Combining the core positions, $s^{x_i}_{j_i}$ and $s^{u_p}_{q_p}$, into vectors yields the core position vectors, $\mathbf{s}^{\mathbf{x}}_{\mathbf{j}}$ and $\mathbf{s}^{\mathbf{u}}_{\mathbf{q}}$, respectively. The combination of the core position derivatives into a vector leads to the core position gradient, $\mathbf{s}^{\dot{\mathbf{x}}}_{\mathbf{w}(\mathbf{j},\mathbf{q})}$.

The membership functions $\mu^{x_i}_{j_i}(x_i)$ have to satisfy the following conditions

(i) Delimitation: $\mu^{x_i}_{j_i}(x_i) \in [0, 1]$ for all $x_i \in X_i$,

(ii) Convexity: $\begin{cases} \mu^{x_i}_{j_i}(x_i) & \text{monotonically increases} \\ & \text{for all } x_i < s^{x_i}_{j_i} \\ \mu^{x_i}_{j_i}(x_i) & \text{monotonically decreases} \\ & \text{for all } x_i > s^{x_i}_{j_i} \end{cases}$,

(iii) Partition: $\sum_{j_i} \mu^{x_i}_{j_i}(x_i) = 1$ for all $x_i \in X_i$, and $\mu^{x_i}_{j_i}(s^{x_i}_{j_i}) = 1$ and $\mu^{x_i}_{j_i}(s^{x_i}_{l_i}) = 0$ for $j_i \neq l_i$,

(iv) Continuity: $\mu^{x_i}_{j_i}(x_i)$ is continuous in X_i.

These conditions should also hold for each membership function $\mu^{u_p}_{q_p}(u_p)$ and their core positions, $s^{u_p}_{q_p}$. In practice, triangular functions and ramp functions are employed as membership functions. Thus, the membership functions $\mu^{x_i}_{j_i}(x_i)$ and $\mu^{u_p}_{q_p}(u_p)$ are completely defined by the core positions $s^{x_i}_{j_i}$ and $s^{u_p}_{q_p}$, respectively. Fig. 6 (a) shows an example for the membership functions that are used to fuzzify the premise and that define the fuzzy sets in the consequent of a linguistic rule.

The core position vectors, $\mathbf{s}^{\mathbf{x}}_{\mathbf{j}} \in X = \mathbb{R}^n$ and $\mathbf{s}^{\mathbf{u}}_{\mathbf{q}} \in U = \mathbb{R}^m$, and the combinations thereof, form a lattice in the state space, X, the input space, U, and the space $X \times U$, respectively. Fig. 6 (b) shows an example. Due to condition 3), there is only one active rule in any core position vector, $(\mathbf{x}, \mathbf{u}) = (\mathbf{s}^{\mathbf{x}}_{\mathbf{j}}, \mathbf{s}^{\mathbf{u}}_{\mathbf{q}})$, such that only one core position gradient, $\mathbf{s}^{\dot{\mathbf{x}}}_{\mathbf{w}(\mathbf{j},\mathbf{q})}$, is associated to each combination $(\mathbf{s}^{\mathbf{x}}_{\mathbf{j}}, \mathbf{s}^{\mathbf{u}}_{\mathbf{q}})$. The core position gradient, $\mathbf{s}^{\dot{\mathbf{x}}}_{\mathbf{w}(\mathbf{j},\mathbf{q})}$, defines the change in the state value with respect to time in the corresponding lattice point, $(\mathbf{s}^{\mathbf{x}}_{\mathbf{j}}, \mathbf{s}^{\mathbf{u}}_{\mathbf{q}})$, i.e., in which direction and how fast a trajectory passes through this lattice point.

Algebraic multiplication is employed as both the aggregation operator and the implication operator, and summation is employed as the accumulation operator. Defuzzification is based on the center of singletons defuzzification (CoS). The choice of these operators leads to a continuous fuzzy function, $\mathbf{f}(\mathbf{x}, \mathbf{u})$.

Under consideration of the conditions above and according to (Adamy and Kempf, 2003; Kempf and Adamy, 2003; Adamy and Flemming, 2006), we obtain the fuzzy function $\mathbf{f}(\mathbf{x}, \mathbf{u})$ with the following analytical form:

$$\dot{\mathbf{x}}(t) = \mathbf{f}(\mathbf{x}(t), \mathbf{u}(t)) = \sum_{\mathbf{j},\mathbf{q}} \mathbf{s}^{\dot{\mathbf{x}}}_{\mathbf{w}(\mathbf{j},\mathbf{q})} \prod_{i=1}^{n} \mu^{x_i}_{j_i}(x_i) \prod_{p=1}^{m} \mu^{u_p}_{q_p}(u_p). \quad (5)$$

The fuzzy function $\mathbf{g}$ is defined similarly.

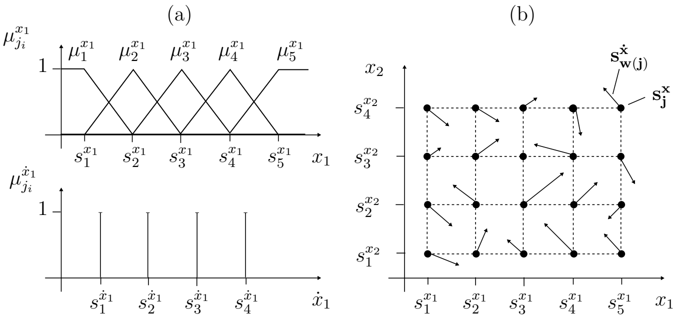

Fig. 6. (a) Examples for the membership functions $\mu_{j_i}^{x_i}(x_i)$ that are used to fuzzify the premise and for the singletons $s_{w_i(\mathbf{j})}^{\dot{x}_i}$ that are used as fuzzy sets in the consequent of a linguistic rule. (b) Example for a lattice in the state space X and recurrent fuzzy system comprising two states and no input.

Note, recurrent fuzzy systems are different from Takagi-Sugeno type fuzzy systems (Adamy and Flemming, 2006). The dynamics of Takagi-Sugeno type fuzzy systems result from the dynamics of local dynamic models, which are fully specified by differential equations and interpolated by using a fuzzy system. An example rule is:

If $x = 1$, then $\dot{x} = Ax + bu$.

In contrast, recurrent fuzzy systems do not interpolate between local dynamic models, but they are based on linguistic rules, which define the dynamics of the system and which use fuzzy sets in the consequent part of each rule, i.e.

If x is "small", then $\dot{x}$ is "positive large".

This leads to dynamics which are inherent to the recurrent fuzzy system. Due to the linguistic definition of the dynamics they are transparent, i.e. interpretable. In general, Takagi-Sugeno type systems do not offer this advantage.

3.2. *Qualitative and quantitative model*

The modeling procedure using continuous-time recurrent fuzzy systems is organized in two steps: Qualitative modeling and quantitative modeling (Adamy and Flemming, 2006).

Step (1): The first step requires at least fuzzy knowledge of the dynamic process in nodes, i.e., by using if-then rules one must be able to describe the state vector, $\mathbf{x}$, and the input vector, $\mathbf{u}$, linguistically by the linguistic vectors, $\mathbf{L}_\mathbf{j}^\mathbf{x}$ and $\mathbf{L}_\mathbf{q}^\mathbf{u}$, and the variation, $\dot{\mathbf{x}}$, of the state vector by the linguistic gradient, $\mathbf{L}_{\mathbf{w(j,q)}}^{\dot{\mathbf{x}}}$, in the nodes $(\mathbf{L}_\mathbf{j}^\mathbf{x}, \mathbf{L}_\mathbf{q}^\mathbf{u})$. The linguistic description of the system dynamics leads to a qualitative model employing if-then rules of the form of (1) or (2).

Step (2): In the second step, measured or representative values have to be assigned to the linguistic model from Step (1). This leads to a quantitative model, which is gained from the qualitative model. The linguistic vectors, $\mathbf{L}_\mathbf{j}^\mathbf{x}$ and $\mathbf{L}_\mathbf{q}^\mathbf{u}$, are represented by numerical values defined as the core position vectors, $\mathbf{s}_\mathbf{j}^\mathbf{x}$ and $\mathbf{s}_\mathbf{q}^\mathbf{u}$, in the state space. Similarly, a core position gradient, $\mathbf{s}_{\mathbf{w(j,q)}}^{\dot{\mathbf{x}}}$, associated with each node $(\mathbf{s}_\mathbf{j}^\mathbf{x}, \mathbf{s}_\mathbf{q}^\mathbf{u})$, numerically represents the linguistic gradient, $\mathbf{L}_{\mathbf{w(j,q)}}^{\dot{\mathbf{x}}}$, in the according node. The derivative, $\dot{\mathbf{x}}$, of the states, $\mathbf{x}$, between the nodes $(\mathbf{s}_\mathbf{j}^\mathbf{x}, \mathbf{s}_\mathbf{q}^\mathbf{u})$ is interpolated using the complete fuzzy system $\mathbf{f}$, which is given by (3).

The two steps of the modeling procedure are shown in Fig. 7.

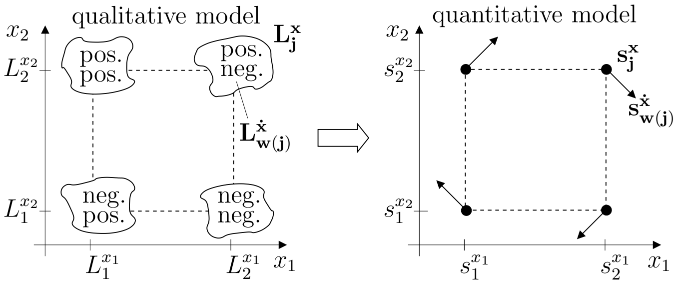

Fig. 7. The qualitative model provides a linguistic description of the dynamics of the system. The quantitative fuzzy model employs numerical values, i.e., the core positions and core position gradients, and interpolates the dynamics in between the core positions.

4. Qualitative Modeling of SOFC

In the following, modeling the electrical behavior of a SOFC, i.e., the dynamical interrelationship between current density J and voltage loss U_V, is accomplished by applying the modeling procedure described in the previous section. The static voltage loss, U_s, and the dynamic voltage loss, U_d, are separately modeled employing the dynamic part (3) and the static part (4) of a continuous-time recurrent fuzzy system, respectively. We start off with the linguistic model.

4.1. *Dynamic Model Part*

The dynamic voltage loss is modeled employing the dynamic model part, $\dot{\mathbf{x}} = \mathbf{f}(\mathbf{x}, \mathbf{u})$, of a recurrent fuzzy system (3), (4). According to Haschka *et al.* (2006), we assume that the two dynamic effects, i.e., the temperature effect and structural effect, are independent of each other. Thus, the two different effects that lead to a dynamic voltage loss are modeled separately. Therefore, we introduce the variable U_{d1} for the dynamic voltage loss that results from the temperature effect and the variable U_{d2} for the dynamic voltage loss arising from the structural effect. The two effects have different time-constants according Section 2.1. The sum of U_{d1} and U_{d2} yields the overall dynamic voltage loss U_d.

The measured data in Fig. 3 and 4 show that the dynamic voltage loss depends on the current density, J, and the change in current density, $\dot{J}$. It is apparent that the higher the current density J is the larger are the dynamic voltage losses U_{d1} and U_{d2} and the faster is their decay rate. Fig. 8 shows a zoomed plot of the measured data where the

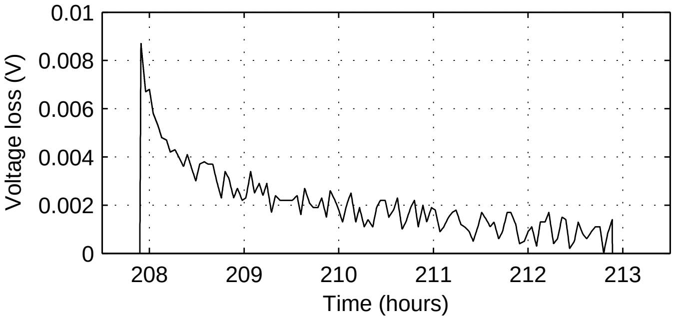

Fig. 8. Zoomed plot of the measured voltage loss, which shows the dynamic part U_d of the overall voltage loss U_V.

Table 1
Linguistic values L_i^J that are used in the qualitative model. The index $i \in \{0, \ldots, 9\}$ indicates the current level in the measured data to which the linguistic values L_i^J belong. *z*="zero", *vt*="very tiny", *t*="tiny", *vs*="very small", *s*="small", *m*="medium", *ml*="medium large", *l*="large", *vl*="very large", *h*="huge."

	i									
	0	1	2	3	4	5	6	7	8	9
L_i^J	z	vt	t	vs	s	m	ml	l	vl	h

dynamic voltage loss, U_d, for a high current density, J, and a positive step in the current density can be observed.

This leads for, e.g., U_{d1} to rules of the form

If $J = L_i^J$ and $\dot{J} = L_k^{\dot{J}}$ and $U_{d1} = L_l^{U_{d1}}$, then $\dot{U}_{d1} = L_{k,l,i}^{\dot{U}_{d1}}$.

The rules for U_{d2} are similar. The current density, J, takes on one linguistic value L_i^J for each current level $i \in \{0, \ldots, 9\}$ of the measured data, which are summarized in Table 1.

Furthermore, the variation of the current density, $\dot{J}$, takes on the linguistic values $L_k^{\dot{J}} \in \{$"negative", "zero", "positive"$\}$ indicated by the index $k \in \{1, 2, 3\}$, respectively, and the voltage loss U_{d1} takes on the linguistic values $L_l^{U_{d1}} \in \{$"negative","zero", "positive"$\}$ indicated by the index $l \in \{1, 2, 3\}$, respectively. The linguistic rules for $\dot{U}_{d1}$ are summarized in Table 2, where the linguistic values $L_{k,l,i}^{\dot{U}_{d1}}$ are given. Note, the rule base in Table 2 is used for each current level $i \in \{0, \ldots, 9\}$. Replacing U_{d1} and $\dot{U}_{d1}$ by U_{d2} and $\dot{U}_{d2}$, respectively, in Table 2, leads to the rule base for the dynamic voltage loss U_{d2}, which arises from the structural effect.

The above described dynamic model part can be represented by

$$\left[\dot{U}_{d1}, \dot{U}_{d2}\right]^T = \mathbf{f}(U_{d1}, U_{d2}, J, \dot{J}), \tag{6}$$

where the function $\mathbf{f}$ is defined according to Section 3.1.

Note, the dynamic part of the qualitative model allows to model U_{d1} and U_{d2} for each current level $i \in \{0, \ldots, 9\}$ separately. This yields $3 \times 3 \times 2$ rules for each current level, such that the model remains transparent, although the overall number of rules is high, i.e., modeling all current levels $i \in \{0, \ldots, 9\}$ leads to $10 \times 3 \times 3 \times 2 = 180$ rules for the dynamic model part. Since the fuzzy system interpolates values between the modeled current levels, it is also possible to reduce the number of rules by modeling the dynamic effects for fewer current levels, which leads to a less complex, but less accurate model. Note, the dynamic voltage losses depend nonlinearly on the current density. This can easily be included into the model since each current level is modeled separately.

Table 2
Rule base that describes the variation $\dot{U}_{d1}$ of the voltage loss U_{d1} for a certain current level L_i^J using the linguistic values $L_{k,l,i}^{\dot{U}_{d1}} \in \{nvl, nl, n, ln, z, lp, p, pl\}$, where *nvl*="negative very large", *nl*="negative large", *n*="negative", *ln*="less negative", *z*="zero", *lp*="less positive", *p*="positive", *pl*="positive large", *pvl*="positive very large."

$\dot{U}_{d1}$		U_{d1}		
		n	z	p
	n	ln	nl	nvl
$\dot{J}$	z	p	z	n
	p	pvl	pl	lp

$$J = L_i^J,\ i \in \{0, \ldots, 9\}$$

Table 3
Rule base that determines the overall voltage loss, U_V, by combining the static voltage loss, U_s, with the dynamic voltage losses, U_{d1} and U_{d2}.

U_V		U_{d1}	
		n	p
U_{d2}	n	$L_{1,1,i}^{U_V}$	$L_{3,1,i}^{U_V}$
	p	$L_{1,3,i}^{U_V}$	$L_{3,3,i}^{U_V}$

$$J = L_i^J,\ i \in \{0, \ldots, 9\}$$

4.2. *Static Model Part*

The overall voltage loss, U_V, depending on the current density, J, and the dynamic voltage losses, U_{d1} and U_{d2}, is described by rules of the form

If $J = L_i^J$ and $U_{d1} = L_l^{U_{d1}}$ and $U_{d2} = L_j^{U_{d2}}$,
then $U_V = L_{l,j,i}^{U_V}$.

The linguistic values $L_{1,1,i}^{U_V}$, $L_{1,3,i}^{U_V}$, $L_{3,1,i}^{U_V}$, and $L_{3,3,i}^{U_V}$ describe the overall voltage loss U_V. The static voltage loss, U_s, does not explicitly occur in these rules. But, U_s depends on the current density, J, and therefore, it is considered implicitly in these rules. In contrast to the dynamic model part, only two linguistic values are used in Table 3 for U_{d1} and U_{d2}, respectively, i.e., $L_1^{U_{d1}}$, $L_3^{U_{d1}}$, $L_1^{U_{d2}}$, and $L_3^{U_{d2}}$, which reduces the number of rules.

The rule base shown in Table 3 is evaluated using the static model part $y = g(\mathbf{x}, \mathbf{u})$ from a recurrent fuzzy system (3), (4). This leads to the representation

$$U_V = g(U_{d1}, U_{d2}, J), \tag{7}$$

where the function g is defined according to Section 3.1.

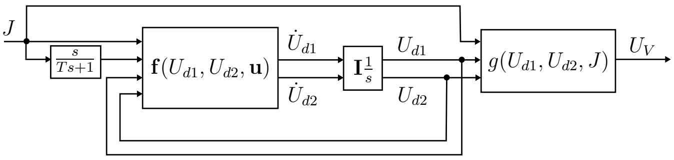

Fig. 9. Structure of the SOFC model using continuous-time recurrent fuzzy systems.

Table 4
Core positions s_i^J for the ith current level with $i \in \{0, \ldots, 9\}$.

	i									
	0	1	2	3	4	5	6	7	8	9
s_i^J	0	0.1012	0.1519	0.2024	0.2530	0.3037	0.3543	0.4049	0.4555	0.5061

This leads for each current level $i \in \{0, \ldots, 9\}$ to $2 \times 2 = 4$ rules, so that incorporating all current levels into $y = g(\mathbf{x}, \mathbf{u})$ yields $10 \times 2 \times 2 = 40$ rules. The complexity of $g(\mathbf{x}, \mathbf{u})$ can also be reduced by decreasing the number of current levels, i, which are incorporated into this part of the model. The maximum number of rules of the complete model comprising $\mathbf{f}$ and g yields $180 + 40 = 220$.

The above described model, i.e., the dynamic model part (6) and the static model part (7), yields the structure of the continuous-time recurrent fuzzy system shown in Fig. 9. The derivative $\dot{J}$ of the current density is computed from the measured data by $\dot{J}(s) = s/(Ts+1)J(s)$, with a small time constant $T = 0.01$h , such that $\dot{J}$ takes on only finite values.

In a further step, core positions and core position derivatives have to be assigned to the linguistic values and linguistic derivatives, so that a quantitative model is derived from the above described qualitative model.

5. Quantitative Modeling: Dynamic Model Part

The membership functions, i.e., the core positions and core position derivatives, for the dynamic model part (6) are determined in the following subsections. In a first step, this is done by a heuristical estimation of the parameter values from the analysis of the measured data without applying a numerical method. This is possible due to the transparency, i.e. interpretability, of the recurrent fuzzy system. In a second step, the parameters are estimated using an evolutionary strategy, but this leads only to a small improvement of the simulation results.

5.1. *Estimation of core positions*

We start off by estimating the core positions s_i^J with $i \in \{0, \ldots, 9\}$, i.e., numerical values that are assigned to the linguistic values L_i^J of the current density, J. They are estimated from the current levels $i \in \{0, \ldots, 9\}$ of the measured data shown in Fig. 3, which leads to the core positions s_i^J shown in Table 4.

Next, the core positions $s_l^{U_{d1}}$ and $s_l^{U_{d2}}$ with $l \in \{1, 2, 3\}$, which correspond to the linguistic values $L_l^{U_{d1}}$ and $L_l^{U_{d2}}$, i.e., "negative", "zero", and "positive", are estimated. By

Table 5
Core positions corresponding to the linguistic values of the dynamic voltage losses U_{d1}, U_{d2}, and the change $\dot{J}$ in current density.

$s_1^{U_{d1}}$	$s_2^{U_{d1}}$	$s_3^{U_{d1}}$	$s_1^{U_{d2}}$	$s_2^{U_{d2}}$	$s_3^{U_{d2}}$	$s_1^{\dot{J}}$	$s_2^{\dot{J}}$	$s_3^{\dot{J}}$
-0.02	0	$+0.02$	-0.02	0	$+0.02$	-2	0	$+2$

investigating the measured data, it is observable that the dynamic voltage loss ranges between -0.02V and $+0.02$V, so that the core positions $s_l^{U_{d1}}$ and $s_l^{U_{d2}}$ are chosen accordingly.

Furthermore, the change $\dot{J}$ in current density is determined to be between $-2\text{A/cm}^2\text{min}$ and $+2\text{A/cm}^2\text{min}$, so that the core positions $s_k^{\dot{J}}$ with $k \in \{1, 2, 3\}$ that correspond to the linguistic values $L_k^{\dot{J}}$, i.e., "negative", "zero", and "positive", of the change $\dot{J}$ in current density, are estimated accordingly. The core positions are summarized in Table 5.

5.2. *Elucidation of core position derivatives*

In the following, we explain how the core position derivatives $s_{k,l,i}^{\dot{U}_{d1}}$ and $s_{k,l,i}^{\dot{U}_{d2}}$ that correspond to the linguistic values $L_{k,l,i}^{\dot{U}_{d1}}$ and $L_{k,l,i}^{\dot{U}_{d2}}$ influence the dynamic behavior of U_{d1} and U_{d2}. This can be considered for the determination of their numerical values. Note, the indices k, l, and i indicate to which core position vectors $(s_k^{\dot{J}}, s_l^{U_{d1}}, s_i^J)$ and $(s_k^{\dot{J}}, s_l^{U_{d2}}, s_i^J)$ the core position derivatives $s_{k,l,i}^{\dot{U}_{d1}}$ and $s_{k,l,i}^{\dot{U}_{d2}}$, respectively, belong.

The core position derivatives $s_{2,3,i}^{\dot{U}_{d1}}$ and $s_{2,1,i}^{\dot{U}_{d1}}$ correspond to the decay rate of a positive or negative dynamic voltage loss U_{d1} if $\dot{J} = 0$. The core position derivatives $s_{3,2,i}^{\dot{U}_{d1}}$ and $s_{1,2,i}^{\dot{U}_{d1}}$ correspond to the peak height of the dynamic voltage loss U_{d1} when a step in the current density occurs, i.e., $\dot{J} > 0$ or $\dot{J} < 0$ while $U_{d1} = 0$. This applies also to the core position derivatives $s_{2,3,i}^{\dot{U}_{d2}}$, $s_{2,1,i}^{\dot{U}_{d2}}$, $s_{3,2,i}^{\dot{U}_{d2}}$, and $s_{1,2,i}^{\dot{U}_{d2}}$ of the voltage loss U_{d2}.

The remaining core position derivatives $s_{k,l,i}^{\dot{U}_{d1}}$ and $s_{k,l,i}^{\dot{U}_{d2}}$, belonging to the core position vectors where not either $\dot{J} = 0$ or $U_{d1} = U_{d2} = 0$, combine the decay rates with the peak heights of the voltage losses U_{d1} and U_{d2}. To reduce the number of parameters, which have to be determined, this combination is achieved by

$$
\begin{aligned}
s_{k,l,i}^{\dot{U}_{d1}} &= s_{k,2,i}^{\dot{U}_{d1}} + s_{2,l,i}^{\dot{U}_{d1}}, \\
s_{k,l,i}^{\dot{U}_{d2}} &= s_{k,2,i}^{\dot{U}_{d2}} + s_{2,l,i}^{\dot{U}_{d2}}, \text{ with } k, l \in \{1, 3\},\ i \in \{0, \ldots, 9\}.
\end{aligned} \tag{8}
$$

$s_{2,l,i}^{\dot{U}_{d1}}$ and $s_{2,l,i}^{\dot{U}_{d2}}$ are the decay rates and $s_{k,2,i}^{\dot{U}_{d1}}$, $s_{k,2,i}^{\dot{U}_{d2}}$ the peak heights of the voltage losses U_{d1} and U_{d2}, respectively, depending on the current level.

This leads to the core position derivatives $s_{k,l,i}^{\dot{U}_{d1}}$ of $\dot{U}_{d1}$ shown in Table 6 for the ith current level. The core position derivatives $s_{k,l,i}^{\dot{U}_{d2}}$ of $\dot{U}_{d2}$ are analogously defined, i.e., replacing U_{d1} and $\dot{U}_{d1}$ by U_{d2} and $\dot{U}_{d2}$, respectively, in Ta-

Table 6
The table shows the core position derivatives $s_{k,l,i}^{\dot{U}_{d1}}$, which belong to the core position vectors $(s_k^{\dot{J}}, s_l^{U_{d1}}, s_i^J)$. The core position derivatives describe the change $\dot{U}_{d1}$ of the dynamic voltage loss U_{d1} depending on the change in current density $\dot{J}$, the current density J, and the dynamic voltage loss U_{d1}.

$\dot{U}_{d1}$		U_{d1}		
		$s_1^{U_{d1}}$	$s_2^{U_{d1}}$	$s_3^{U_{d1}}$
	$s_1^{\dot{J}}$	$s_{1,1,i}^{\dot{U}_{d1}} = s_{1,2,i}^{\dot{U}_{d1}} + s_{2,1,i}^{\dot{U}_{d1}}$	$s_{1,2,i}^{\dot{U}_{d1}}$	$s_{1,3,i}^{\dot{U}_{d1}} = s_{1,2,i}^{\dot{U}_{d1}} + s_{2,3,i}^{\dot{U}_{d1}}$
$\dot{J}$	$s_2^{\dot{J}}$	$s_{2,1,i}^{\dot{U}_{d1}}$	$s_{2,2,i}^{\dot{U}_{d1}} = 0$	$s_{2,3,i}^{\dot{U}_{d1}}$
	$s_3^{\dot{J}}$	$s_{3,1,i}^{\dot{U}_{d1}} = s_{3,2,i}^{\dot{U}_{d1}} + s_{2,1,i}^{\dot{U}_{d1}}$	$s_{3,2,i}^{\dot{U}_{d1}}$	$s_{3,3,i}^{\dot{U}_{d1}} = s_{3,2,i}^{\dot{U}_{d1}} + s_{2,3,i}^{\dot{U}_{d1}}$

$J = s_i^J,\ i \in \{0, \dots, 9\}$

ble 6 leads to the rule base for $\dot{U}_{d2}$. Note, the core position derivatives differ for each $i \in \{0, \dots, 9\}$.

5.3. *Estimation of the core position derivatives*

In the following, numerical values are estimated heuristically for all core position derivatives $s_{k,l,i}^{\dot{U}_{d1}}$ and $s_{k,l,i}^{\dot{U}_{d2}}$. The core position derivatives $s_{2,1,i}^{\dot{U}_{d1}}$, $s_{2,3,i}^{\dot{U}_{d1}}$, $s_{2,1,i}^{\dot{U}_{d2}}$, and $s_{2,3,i}^{\dot{U}_{d2}}$, which correspond to the decay rates of U_{d1} and U_{d2}, are estimated by observing the measured data where $\dot{J} = 0$. This leads to the core position derivatives

$$s_{2,1,i}^{\dot{U}_{d1}} = 0.0050\frac{\mathrm{V}}{\mathrm{h}},\ s_{2,3,i}^{\dot{U}_{d1}} = -0.0080\frac{\mathrm{V}}{\mathrm{h}}, \tag{9}$$

$$s_{2,1,i}^{\dot{U}_{d2}} = 0.2000\frac{\mathrm{V}}{\mathrm{h}},\ s_{2,3,i}^{\dot{U}_{d2}} = -0.2000\frac{\mathrm{V}}{\mathrm{h}}, \tag{10}$$

where $i \in \{0, \dots, 9\}$, that yield good simulation results.

The core position derivatives $s_{1,2,i}^{\dot{U}_{d1}}$, $s_{3,2,i}^{\dot{U}_{d1}}$, $s_{1,2,i}^{\dot{U}_{d2}}$, and $s_{3,2,i}^{\dot{U}_{d2}}$, which model the peak height of U_{d1} and U_{d2} for a step in the current density J, are estimated using the measured data where $\dot{J} > 0$ or $\dot{J} < 0$ while $U_{d1} \approx 0$ and $U_{d2} \approx 0$. This yields the heuristically estimated values for the core position derivatives on the current levels $i \in \{0, 3, \dots, 9\}$ shown in Table 7.

Note, due to the interpolating character of the fuzzy system, it is not necessary to model the dynamics for all current levels $i \in \{0, \dots, 9\}$. Thus, the small dynamics for $i = \{1, 2\}$ are not modeled separately, but the fuzzy system interpolates these dynamics between the dynamics on the current level $i = 0$ and $i = 3$. The remaining core position derivatives are calculated by inserting the values from (9), (10), and Table 7 into Table 6.

Considering the dynamic model part incorporating the current levels $i \in \{0, 3, \dots, 9\}$, Fig. 10 shows example maps of $\dot{U}_{d1}$ and $\dot{U}_{d2}$ depending on the current density, J, and the change in current density, $\dot{J}$. Fig. 11 shows similar maps of $\dot{U}_{d1}$ and $\dot{U}_{d2}$ depending on the current density, J, and the voltages U_{d1} and U_{d2}, respectively.

Table 7
Heuristically estimated core position derivatives $s_{1,2,i}^{\dot{U}_{d1}}$, $s_{3,2,i}^{\dot{U}_{d1}}$, $s_{1,2,i}^{\dot{U}_{d2}}$, and $s_{3,2,i}^{\dot{U}_{d2}}$ for the ith current level with $i \in \{0, 3, \dots, 9\}$ of the current density J. For $i \in \{1, 2\}$ the dynamics are small, so that it is not necessary to model these current levels.

	i							
	0	3	4	5	6	7	8	9
$s_{1,2,i}^{\dot{U}_{d1}}$	0.0000	-0.1300	-0.1300	-0.1300	-0.1300	-0.1300	-0.1400	-0.1400
$s_{3,2,i}^{\dot{U}_{d1}}$	0.0000	0.0400	0.1500	0.1500	0.1500	0.1500	0.1500	0.1500
$s_{1,2,i}^{\dot{U}_{d2}}$	0.0000	0.0000	0.0000	-0.0200	-0.0600	-0.1200	-0.1400	-0.1400
$s_{3,2,i}^{\dot{U}_{d2}}$	0.0000	0.0000	0.0000	0.0200	0.0300	0.0600	0.0800	0.3000

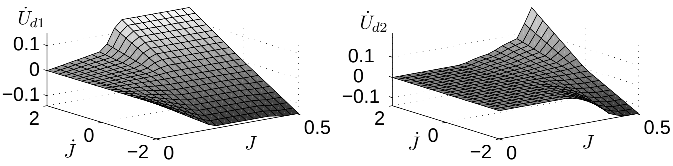

Fig. 10. Maps of the change in voltage losses, $\dot{U}_{d1}$ and $\dot{U}_{d2}$, depending on the current density, J, and the change in current density, i.e., depending on $J = s_i^J$ and $\dot{J} = s_i^{\dot{J}}$, with $i \in \{0, 3, \dots, 9\}$. Here, $U_{d1} = U_{d2} = 0$.

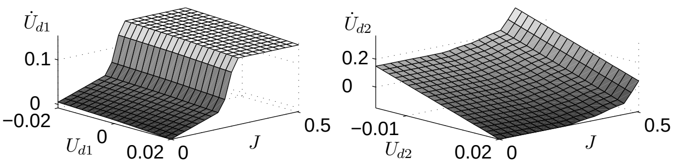

Fig. 11. Maps of the change in voltage loss, $\dot{U}_{d1}$ and $\dot{U}_{d2}$, depending on the voltage losses U_{d1} and U_{d2}, respectively and the current density, J, i.e., $J = s_i^J$, with $i \in \{0, 3, \dots, 9\}$. Here, $\dot{J} = 2A/cm^2s$.

6. Quantitative Modeling: Static Model Part

The summation of the dynamic voltage losses, U_{d1} and U_{d2}, with the static voltage loss, U_s, leads to the overall voltage loss $U_V = U_{d1} + U_{d2} + U_s$. This is considered when estimating the core positions $s_{1,1,i}^{U_V}$, $s_{1,3,i}^{U_V}$, $s_{3,1,i}^{U_V}$, and $s_{3,3,i}^{U_V}$, i.e., the membership functions, that correspond to the linguistic values $L_{1,1,i}^{U_V}$, $L_{1,3,i}^{U_V}$, $L_{3,1,i}^{U_V}$, and $L_{3,3,i}^{U_V}$ of the static model part (7). To reduce the number of parameters, which have to be estimated, the core positions $s_{l,j,i}^{U_V}$ corresponding to the linguistic values $L_{l,j,i}^{U_V}$ of U_V are estimated according to

$$s_{l,j,i}^{U_V} = s_l^{U_{d1}} + s_j^{U_{d2}} + U_s(i) \tag{11}$$

with $l, j \in \{1, 3\}$ and $i \in \{0, \dots, 9\}$. $U_s(i)$ corresponds to the static voltage loss that occurs on the ith current level and is read off from the measured data in Fig. 4. $s_l^{U_{d1}}$ and $s_j^{U_{d2}}$ are the core positions of U_{d1} and U_{d2}, respectively. Using (11) for all core positions $s_{l,j,i}^{U_V}$ leads to a rule base that corresponds to $U_V = U_{d1} + U_{d2} + U_s$. The resulting rule base is shown in Table 8.

Note, only the values $U_s(i)$ have to be estimated for each current level $i \in \{0, \dots, 9\}$. They are given in Table 9. The values for $s_l^{U_{d1}}$ and $s_j^{U_{d2}}$ are the same as in the dynamic model part, which are given in Table 5. Using Tables 5 and 9 the numerical values in Table 8 are calculated.

Table 8
The table shows the rule base that describe the overall voltage loss, U_V, depending on the current density, J, the static voltage loss, U_s, and the dynamic voltage losses, U_{d1} and U_{d2}.

U_V		U_{d1}	
		$s_1^{U_{d1}}$	$s_3^{U_{d1}}$
U_{d2}	$s_1^{U_{d2}}$	$s_{1,1,i}^{U_V} = s_1^{U_{d1}} + s_1^{U_{d2}} + U_s(i)$	$s_{3,1,i}^{U_V} = s_3^{U_{d1}} + s_1^{U_{d2}} + U_s(i)$
	$s_3^{U_{d2}}$	$s_{1,3,i}^{U_V} = s_1^{U_{d1}} + s_3^{U_{d2}} + U_s(i)$	$s_{3,3,i}^{U_V} = s_3^{U_{d1}} + s_3^{U_{d2}} + U_s(i)$
		$J = s_i^J$, $i \in \{0, \ldots, 9\}$	

Table 9
Static voltage $U_s(i)$ for the ith current level with $i \in \{0, \ldots, 9\}$.

	i									
	0	1	2	3	4	5	6	7	8	9
$U_s(i)$	0	0.0560	0.0890	0.1174	0.1412	0.1634	0.1849	0.2067	0.2289	0.2510

Instead of heuristically estimating the parameters of the dynamic and static model part, they can also be identified numerically. Therefore, the parameters of the model, which are numerically optimized, are combined into a parameter vector

$$\mathbf{p} = [\mathbf{p}_0, \ldots, \mathbf{p}_9, U_s(1), \ldots, U_s(9)]^T, \text{ where}$$
$$\mathbf{p}_i = [s_{2,1,i}^{\dot{U}_{d1}}, s_{2,3,i}^{\dot{U}_{d1}}, s_{1,2,i}^{\dot{U}_{d1}}, s_{3,2,i}^{\dot{U}_{d1}}, s_{2,1,i}^{\dot{U}_{d2}}, s_{2,3,i}^{\dot{U}_{d2}}, s_{1,2,i}^{\dot{U}_{d2}}, s_{3,2,i}^{\dot{U}_{d2}}] \tag{12}$$

for all $i \in \{0, \ldots, 9\}$. Note, only the parameters that are actually incorporated into the model are combined into the parameter vector, e.g., if the current levels $i \in \{0, 3, \ldots, 9\}$ are incorporated into the dynamic model part, only $\mathbf{p}_i$ with $i \in \{0, 3, \ldots, 9\}$ are considered. By minimizing the quadratic cost function

$$F(\mathbf{p}, t) = \int_0^t (U_{V,measured}(\tau) - U_{V,model}(\tau, \mathbf{p}))^2 d\tau \tag{13}$$

using an evolutionary strategy, a parameter set that further enhances the model accuracy can numerically be determined.

7. Time-Invariant Model: Simulation Results

Due to the interpolating character of the fuzzy system, it is not necessary to incorporate all core positions s_i^J with $i \in \{0, \ldots, 9\}$ into the model to obtain accurate simulation results. In the following, we consider several model configurations, which differ in the number of core positions that are used in the dynamic model part. In each model configuration, the static model part comprises all current levels $i \in \{0, \ldots, 9\}$, since the complexity of the static model part is low. The model incorporating the current levels $i \in \{0, 3, \ldots, 9\}$ in the dynamic model part is denoted 03-9-model.

Analogously, we introduce a 09-model and a 069-model, which incorporate the current levels $i \in \{0, 9\}$ and $i \in \{0, 6, 9\}$, respectively. These models are less complex than the 03-9-model, and in return, some accuracy is lost. Either the parameters determined in Section 4 can be used

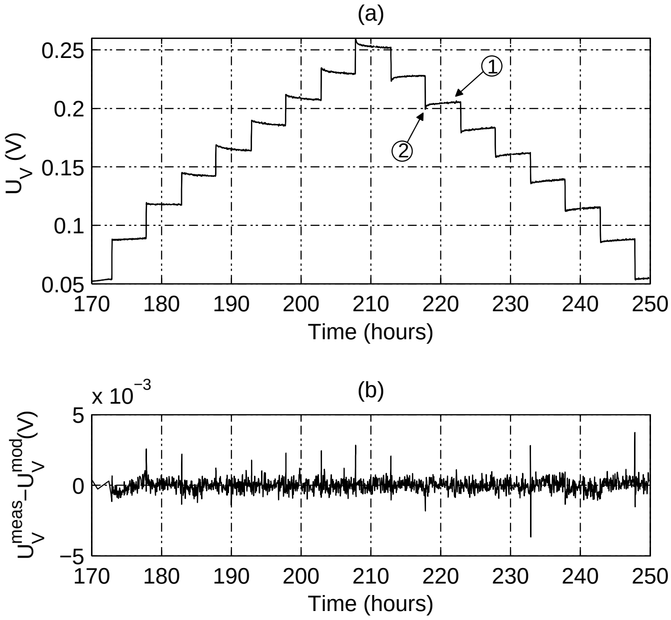

Fig. 12. (a) Plot of the measured voltage loss (1) and the modeled voltage loss (2) using the 03-9-model. (b) Difference between the measured voltage loss U_V^{meas} and the modeled voltage loss U_V^{mod}.

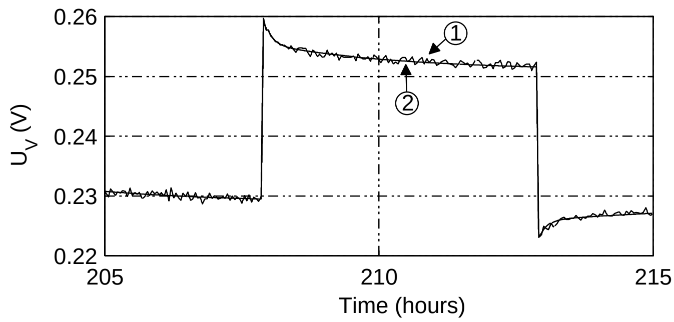

Fig. 13. Zoomed plot of the measured voltage loss (1) and the modeled voltage loss (2) using the 03-9-model.

for all three model configurations or numerically identified parameters can be determined using (13).

The results, obtained by the 03-9-model with the heuristically determined model parameters from Section 4 are shown in Fig. 12, 13. The difference between measurement and simulation mainly results mainly from the measurement noise. Fig. 14 shows a zoomed plot of the simulated dynamic voltage losses U_{d1}, U_{d2}, and the overall dynamic voltage loss U_d in comparison to the measured dynamic voltage loss from Fig. 8. Note, these plots show that this model yields accurate estimations of the voltage loss U_V, such that there exists almost no difference between the measurement and the simulation. Thus, the presented qualitative and quantitative model is appropriate.

Fig. 15 shows the root mean square of the relative model error, $RMS(\mathbf{p}, t)$, of the models with heuristically estimated parameters compared to the 03-9-model with numerically identified parameters. As one expects, the more core positions, i.e., the more rules, are incorporated into the model, the more accurate is the simulation result. Note,

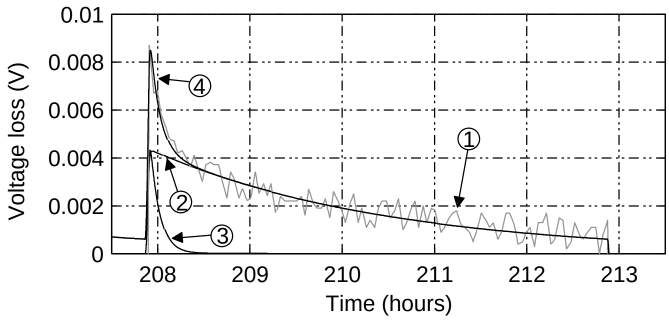

Fig. 14. Plot of (1) the dynamic part of the measured voltage loss $U_V - U_s(9)$, (2) the modeled dynamic voltage loss U_{d1}, (3) the modeled dynamic voltage loss U_{d2}, and (4) the modeled dynamic voltage loss U_d using the 03-9-model.

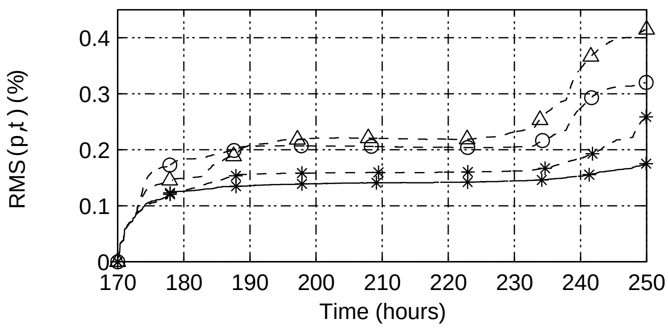

Fig. 15. Root mean square of the relative model error, $RMS(\mathbf{p}, t)$, depending on the simulation time t. The symbols are: $\triangle$ =09-model, $\bigcirc$ =069-model, $\star$ =03-9-model. The dashed lines show the evolution of the cost function with the heuristically determined parameters, while the solid line represents the evolution with the optimized parameters.

the 03-9-model with heuristically chosen parameters is almost as accurate as the 03-9-model with numerical identified parameters. This is possible due to the transparency of the model, which allows the accurate estimation of the parameters.

In Table 10 the values of $RMS(\mathbf{p}, t)$ for $t = 250$h are shown for the heuristically, $\mathbf{p}_{heu}$, and numerically, $\mathbf{p}_{num}$, determined model parameters. The 03-9-model with the numerically determined parameters achieves the highest accuracy, since it incorporates more current levels i than the 069-model and the 09-model. A model which includes all current levels 0-9 is not shown in the table. It leads only to a very slight improvement of the simulation results in comparison to the 03-9-model, since there are only very small dynamics on the current levels 1-2. Thus, they can be interpolated between the very small dynamics on the current levels zero and three. Incorporating the current levels 1-2 only increases the number of rules, which is disadvantageous. However, all model configurations yield accurate simulation results.

In Haschka *et al.* (2006) a switching Hammerstein-model with an additive nonlinearity was proposed to model the voltage loss during operation of a SOFC. The simulation results of the proposed time-invariant model and the model in Haschka *et al.* (2006) are both similar accurate.

Table 10
Values of the root mean square of the relative model error, $RMS(\mathbf{p}, t)$, at time $t = 250$h for heuristically, $\mathbf{p}_{heu}$, and numerically, $\mathbf{p}_{num}$, determined model parameters. The results are shown for models incorporating a different number of current levels s_i^J into the dynamic model part, i.e., $03 - 9$: $i \in \{0, 3, \ldots, 9\}$, 069: $i \in \{0, 6, 9\}$, and 09: $i \in \{0, 9\}$.

	Model		
	$03 - 9$	069	09
$RMS(\mathbf{p}_{heu})$ [%]	0.26	0.32	0.42
$RMS(\mathbf{p}_{num})$ [%]	0.18	0.21	0.20

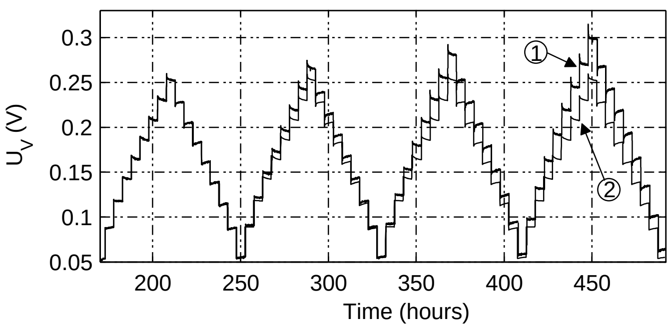

Fig. 16. Voltage loss U_V, simulated with the time-invariant model (2) compared to the data (1) for a long time simulation. Note, the time-invariant model leads to accurate simulation results during a period of 80 hours. For a long time simulation the deterioration of the SOFC has to be considered.

Unfortunately, a numerical comparison is not feasible, since no numerical error measures are given in Haschka *et al.* (2006). However, the model, using continuous-time recurrent fuzzy systems, is transparent, i.e., interpretable, whereas the switching Hammerstein-model is not.

The model above does not consider the deterioration of a SOFC described in Section 2.2, so that the simulation for a long time period leads to the results shown in Fig. 16. Obviously, the incorporation of the fuel cell deterioration into the model is required to achieve accurate results for the long time simulation.

8. Modeling the Deterioration of the SOFC

The incorporation of the degradation effects into the model is achieved by introducing the additional linguistic state "age", A, into the above introduced nonlinear time-invariant model, which represents the grade of degradation.

The dynamic voltage loss caused by the structural effect, i.e., a positive or negative value of U_{d1}, highly influences the degradation, i.e., the linguistic state A. Furthermore, the current density also influences the degradation process, i.e., a medium value of the current density, J, has a higher influence on the degradation process than a large or a zero current density, so that the current density is also incorporated. The rule base that describes $\dot{A}$ depending on A, J, and U_{d1} is summarized in Table 11.

In this rule base, the two linguistic values

$L_1^A = $ "young", $L_2^A = $ "old",

Table 11
Rule base of the fuel cell degradation. The rules linguistically describe the change $\dot{A}$ in the age A of the fuel cell.

$\dot{A}$		J		
		"zero"	"medium"	"large"
A	"young"	"zero"	"small"	"zero"
	"old"	"zero"	"large"	"zero"

U_{d1} ="positive"

$\dot{A}$		J		
		"zero"	"medium"	"large"
A	"young"	"zero"	"very small"	"zero"
	"old"	"zero"	"medium"	"zero"

U_{d1} ="negative"

describing the state A, are introduced. The two linguistic values represent "no deterioration" and "complete deterioration", respectively. Depending on the current density, J, and the voltage loss U_{d1}, the value of A increases with different rates or is constant. Thus, we introduce the linguistic values

$$L_1^{\dot{A}} = \text{"zero"},\ L_2^{\dot{A}} = \text{"very small"},\ L_3^{\dot{A}} = \text{"small"},$$
$$L_4^{\dot{A}} = \text{"medium"},\ L_5^{\dot{A}} = \text{"large"}$$

that describe the derivative $\dot{A}$ of the linguistic state A. The current density, J, and the voltage loss U_{d1} are described by the linguistic values

$$\widetilde{L}_1^J = \text{"zero"},\ \widetilde{L}_2^J = \text{"medium"},\ \widetilde{L}_3^J = \text{"large"},$$
$$\widetilde{L}_1^{U_{d1}} = \text{"negative"},\ \widetilde{L}_2^{U_{d1}} = \text{"positive"},$$

respectively. The dynamic model for A is represented by

$$\dot{A} = f_{Age}(A, U_{d1}, J). \tag{14}$$

The age, A, of the fuel cell influences both the static and dynamic voltage losses that occur during operation. In fact, the linguistic variable A must be integrated into the time-invariant model (6), (7), which requires additional linguistic rules.

Since A takes on the two values L_1^A ="young" and L_2^A ="old", this is achieved by simply using the rule base of the time-invariant model for both L_1^A ="young" and L_2^A ="old" but with different parameters, i.e., with different core positions. The rules of the dynamic model part incorporating A have the following form:

If $A = L_1^A$ and $J = L_i^J$ and $\dot{J} = L_k^{\dot{J}}$
and $U_{d1} = L_l^{U_{d1}}$, then $\dot{U}_{d1} = L_{k,l,i,A0}^{\dot{U}_{d1}}$.

The rules of the static model part have the form

If $A = L_1^A$ and $J = L_i^J$ and $U_{d1} = L_l^{U_{d1}}$
and $U_{d2} = L_j^{U_{d2}}$, then $U_V = L_{l,j,i,A0}^{U_V}$.

These rules lead to

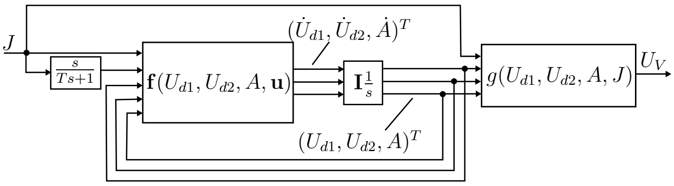

Fig. 17. Structure of the SOFC model incorporating the deterioration A of the fuel cell.

$$\left[\dot{U}_{d1}, \dot{U}_{d2}\right]^T = \mathbf{f}_{U_d A}(U_{d1}, U_{d2}, A, J, \dot{J}), \tag{15}$$
$$U_V = g_A(U_{d1}, U_{d2}, A, J). \tag{16}$$

Combining (14), (15), (16) yields the continuous-time recurrent fuzzy system

$$\left[\dot{U}_{d1}, \dot{U}_{d2}, \dot{A}\right]^T = [\mathbf{f}_{U_d A}, f_{Age}]^T = \mathbf{f}_A(U_{d1}, U_{d2}, A, J, \dot{J}), \tag{17}$$
$$U_V = g_A(U_{d1}, U_{d2}, A, J). \tag{18}$$

Note, since the nonlinear time-invariant model has been incorporated into the time-variant model, the time-variant model is also nonlinear. The nonlinearity results from the nonlinear dependence between the dynamic voltage losses and the current density. The model structure is shown in Fig. 17, where $T = 0.01h$.

The core positions $s_l^{U_{d1}}$, $s_l^{U_{d2}}$, s_i^J, and $s_i^{\dot{J}}$ are chosen to be the same as in the time-invariant case. The core positions s_a^A, $\tilde{s}_i^J$, and $\tilde{s}_l^{U_{d1}}$ are chosen heuristically. The age is measured in %, since the deterioration of the fuel cell depends not only on the operation time, but also on the operation mode. The current density and a change in the current density result in a deterioration of the fuel cell, which cannot be measured in time. It is only possible to say that there is no deterioration (0%) or the deterioration increases until the fuel cell is completely deteriorated (100%). Thus, the core positions s_a^A are chosen to be $s_1^A = 0\%$ and $s_2^A = 100\%$ to represent the linguistic values "young" and "old", i.e. no deterioration or complete deterioration of the fuel cell, respectively. The remaining core positions and core position derivatives in the time-variant model are determined by applying a numerical optimization method. Therefore, they are combined into a parameter vector, $\mathbf{p}_A$. Minimizing the cost function (13) with respect to the parameter vector $\mathbf{p}_A$ by using an evolutionary strategy yields the core positions and the core position derivatives. The values are given in the appendix.

9. Time-Variant Model: Simulation Results

In the following, the simulation results, which are achieved using the time-variant model incorporating the deterioration of the fuel cell, are presented. The results for a 03-9-model, where the dynamic model part incorporates the current levels s_i^J with $i \in \{0, 3, \dots 9\}$ and the static model part employs all current levels s_i^J with $i \in \{0, \dots, 9\}$, are shown.

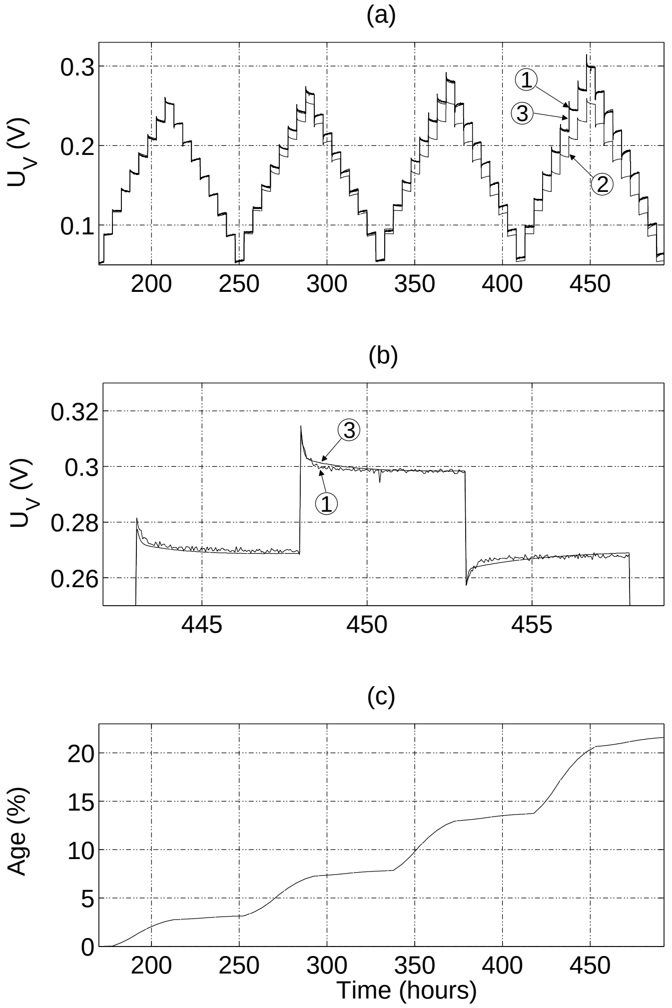

Fig. 18. (a) Voltage loss U_V, simulated with the time-variant model (3) and with the time-invariant model (2) compared to the data (1). Note, the time-variant model yields an accurate estimation of the voltage loss U_V, such that there is no difference observable to the measured data. (b) Zoom of U_V simulated with the time-variant model (3) compared to the measured data (1). (c) The deterioration, i.e., the age A, of the fuel cell model is shown.

Fig. 18 (a) shows the estimation of the voltage loss U_V using the time-variant model in comparison to the time-invariant model and the measured data. In contrast to the time-invariant model, which allows accurate simulations over a period of approximately 80 hours, the simulation using the time-variant model accurately estimates the voltage loss over a period of approximately 320 hours. During this period, the simulation results are almost identical with the measured data. A zoom of the plot presented in Fig. 18 (b) shows the accuracy of the simulated voltage loss U_V using the time-variant model. The root mean square of the relative model error yields at time $t = 492$h a value of $RMS(\mathbf{p}_{num}) = 0.75\%$. Furthermore, the time-variant model allows assessing the grade of deterioration of the fuel cell, which can be observed in Fig. 18 (c).

In contrast to our proposed time-variant model, where we modify the characteristics of U_{d1}, U_{d2}, and U_s to incorporate the deterioration of the fuel cell, the time-variant model in Haschka *et al.* (2006) modifies only the characteristics of U_s. Thus, the simulation results are similar accurate considering the static voltage loss, but they differ considering the dynamic voltage loss. The measured data shows that the dynamic voltage loss depends on the deterioration. Thus, if a higher accuracy is necessary for the dynamic voltage losses, the proposed model is beneficial.

Table 12
Rule base for the linguistic derivative $\dot{A}$.

$\dot{A}$		J 0	0.3	0.6
A	0	0	0.1	0
	100	0	1.21	0

$U_{d1} = 1 \cdot 10^{-5}$

$\dot{A}$		J 0	0.3	0.6
A	0	0	0.0107	0
	100	0	0.1296	0

$U_{d1} = -1 \cdot 10^{-5}$

Table 13
Numerical values for the static voltage loss $U_{s,A0}(i)$ and $U_{s,A100}(i)$.

i	0	1	2	3	4	5	6	7	8	9
$U_{s,A0}(i)$	0	0.0559	0.0899	0.1153	0.1396	0.1621	0.1836	0.2045	0.2258	0.2473
$U_{s,A100}(i)$	0	0.1107	0.1664	0.2323	0.2790	0.3249	0.3658	0.4138	0.4462	0.5029

10. Conclusions

This work presents an approach to model the dynamic current density/voltage loss characteristics of a SOFC using continuous-time recurrent fuzzy systems. A time-invariant and a time-variant model have been developed, which allow accurate simulations. The advantage of the proposed models in comparison to models that are found in literature are their transparency and interpretability. Thus, comprehensible and accurate models are proposed for the dynamic simulation of the current density/voltage loss characteristics of a SOFC. The model is also applicable to other types of fuel cells by modifying the model parameters, since the effects that cause static and dynamic voltage losses, occur also in other types of fuel cells.

11. Acknowledgment

The authors thank V. Krebs, University of Karlsruhe, Germany, who supported this work. We also thank T. Lens and E. Lenz for their support concerning the simulation and optimization parts.

12. Appendix

The parameters that are used to determine the core positions and core position derivatives of the model incorporating the deterioration of the fuel cell, are given in Tables 12, 13, and 14. The values for the core positions $s_l^{U_{d1}}$, $s_l^{U_{d2}}$, s_i^{J}, and $s_i^{\dot{J}}$ of U_{d1}, U_{d2}, J, and $\dot{J}$, respectively, which are used in the time-variant model are the same as for the time-invariant model given in Tables 4, 5.

Table 14
Core position derivatives for the dynamic voltage losses U_{d1} and U_{d2}.

	i							
	0	3	4	5	6	7	8	9
$s^{\dot{U}_{d1}}_{1,2,i,A0}$	0.0000	-0.0957	-0.1298	-0.1593	-0.1160	-0.1846	-0.1817	-0.0987
$s^{\dot{U}_{d1}}_{3,2,i,A0}$	0.0000	0.1090	0.2983	0.1930	0.2000	0.1717	0.1646	0.0912
$s^{\dot{U}_{d1}}_{2,1,i,A0}$	0.0053	0.0021	0.0020	0.0044	0.0008	0.0034	0.0047	0.0053
$s^{\dot{U}_{d1}}_{2,3,i,A0}$	-0.0112	-0.0008	-0.0058	-0.0064	-0.0048	-0.0059	-0.0055	-0.0098
$s^{\dot{U}_{d2}}_{1,2,i,A0}$	0.0000	0.0000	0.0000	-0.0140	-0.0074	-0.1043	-0.1352	-0.3413
$s^{\dot{U}_{d2}}_{3,2,i,A0}$	0.0000	0.0000	0.0000	0.0188	0.0371	0.0786	0.0920	0.2589
$s^{\dot{U}_{d2}}_{2,1,i,A0}$	0.1579	0.2184	0.1170	0.1170	0.2959	0.0936	0.1344	0.1508
$s^{\dot{U}_{d2}}_{2,3,i,A0}$	-0.2266	-0.1409	-0.0825	-0.0343	-0.2749	-0.1174	-0.0725	-0.1577
$s^{\dot{U}_{d1}}_{1,2,i,A100}$	0.0000	-0.7779	-0.6730	-0.9629	-0.5346	-0.4563	-0.5935	-0.9222
$s^{\dot{U}_{d1}}_{3,2,i,A100}$	0.0000	0.0559	0.0689	0.3021	0.5979	0.1459	0.2477	0.9142
$s^{\dot{U}_{d1}}_{2,1,i,A100}$	0.0203	0.0011	0.0183	0.0144	0.0237	0.0273	0.0230	0.0104
$s^{\dot{U}_{d1}}_{2,3,i,A100}$	-0.0120	-0.0186	-0.0135	-0.0018	-0.0160	-0.0130	-0.0325	-0.0212
$s^{\dot{U}_{d2}}_{1,2,i,A100}$	0.0000	0.0000	0.0000	-0.1900	-0.4361	-1.6988	-1.2632	-1.9208
$s^{\dot{U}_{d2}}_{3,2,i,A100}$	0.0000	0.0000	0.0000	0.0930	0.2612	0.1674	1.7343	2.3481
$s^{\dot{U}_{d2}}_{2,1,i,A100}$	1.3280	1.5768	1.1101	0.8143	1.4201	2.0645	2.0045	0.9561
$s^{\dot{U}_{d2}}_{2,3,i,A100}$	-1.3412	-1.1347	-1.6153	-1.6566	-1.8498	-0.3047	-1.0478	-0.9750

References

Achenbach, E. (1995). Response of a solid oxide fuel cell to load change. *J. Power Sources* **57**, 105–109.

Adamy, J. (1995). Device for early detection of runout in continuous casting. EP Priority Date 03.04.1995, European Patent 0819033B1 (1998), US Patent 5,904,202 (1999).

Adamy, J. and A. Flemming (2006). Equilibria of continuous-time recurrent fuzzy systems. *Fuzzy Sets and Systems* **157**(22), 2913–2933.

Adamy, J. and R. Kempf (2003). Regularity and chaos in recurrent fuzzy systems. *Fuzzy Sets and Systems* **140**(2), 259–284.

Adamy, J. and R. Kempf (2004). A survey on fuzzy systems with inherent dynamics. *Automatisierungstechnik* **52**(10), 459–469. (in German).

Badard, R. and T. Pontet (1997). Continuous interpolation logic and qualitative modeling of flows. *Fuzzy Sets and Systems* **85**(3), 355–371.

di Sciascio, F. and R. Carelli (1996). Fuzzy modelling and identification of multilinear dynamical systems. In: *FUZZ-IEEE 96, Proc. of 5th International Conference on Fuzzy Systems.* number 2. IEEEE. New Orleans, USA. pp. 848–854.

Gemmen, R.S. and C.D. Johnson (2005). Effect of load transients on sofc operation - current reversal on loss of load. *J. Power Sources* **144**, 152–164.

Gorrini, V. and H. Bersini (1994). Recurrent fuzzy systems. In: *Proc. 3rd IEEE Conf. on Fuzzy Systems.* Vol. 1. Orlando, USA. pp. 193–198.

Hall, D.J. and R.G. Colclaser (1999). Transient modeling and simulation of a tubular solid oxide fuel cell. *IEEE Trans. Energy Convers.* **14**(3), 749–753.

Haschka, M., T. Weickert, V. Krebs, S. Schfer and E. Ivers-Tiffée (2006). Identification of a nonlinear model for the electrical behavior of a solid oxide fuel cell. *J. Power Sources* **156**(1), 71–77.

Ivers-Tiffée, E., A. Weber, K. Schmid and V. Krebs (2004). Macroscale modeling of cathode formation in sofc. *Solid State Ionics* **174**, 223–232.

Jurado, F. (2004*a*). Modeling sofc plants on the distribution system using identification algorithms. *J. Power Sources* **129**, 205–215.

Jurado, F. (2004*b*). Nonlinear model identification of fuel cell power plant. In: *Proc. 7th IEEE AFRICON.* Vol. 2. Gaborone, Botswana. pp. 769–774.

Jurado, F., J.R. Saenz and L. Fernández (2004). Modeling fuel cell plants on the distribution system using identification algorithms. In: *Proc. IEEE 12th MELECON.* Dubrovnik, Croatia.

Kempf, R. and J. Adamy (2003). Equilibria of recurrent fuzzy systems. *Fuzzy Sets and Systems* **140**(2), 231–257.

Larminie, J. and A. Dicks (2003). *Fuel Cell Systems Explained.* Wiley. Hoboken, USA.

Lu, N., Q. Li, X. Sun and M.A. Khaleel (2006). The modeling of a standalone solid-oxide fuel cell auxiliary power unit. *J. Power Sources.* in press.

O'Hayre, R., S.-W. Cha, W. Colella and F.B. Prinz (2006). *Fuel cell fundamentals.* Wiley. Hoboken, USA.

Ota, T., M. Koyama, C.-j. Wen, K. Yamada and H. Takahashi (2003). Object-based modeling of sofc system: dynamic behavior of micro-tube sofc. *J. Power Sources* **118**, 430–439.

Padullé, J., G.W. Ault and J.R. McDonald (2000). An integrated sofc plant dynamic model for power systems simulation. *J. Power Sources* **86**, 495–500.

Qi, Y., B. Huang and J. Luo (2006). Nonlinear state space modeling and simulation of a sofc fuel cell. In: *Proc. 2006 IEEE American Control Conf..* Minneapolis, USA. pp. 2534–2538.

Qi, Y., B. Huang and K.T. Chuang (2005). Dynamic modeling of solid oxide fuel cell: The effect of diffusion and inherent impedance. *J. Power Sources* **150**, 32–47.

Sedghisigarchi, K. and A. Feliachi (2004). Dynamic and transient analysis of power distribution systems with fuel cells - part I: Fuel-cell dynamic model. *IEEE Trans. Energy Convers.* **19**(2), 423–428.

Xu, M., C. Wang, Y. Qiu, B. Lu, F.C. Lee and G. Kopasakis (2006). Control and simulation for hybrid solid oxide fuel cell power systems. In: *Proc. 21st IEEE APEC '06.* Dallas, USA. pp. 1269–1274.